Revision Unmarked

Polar-Facing Slopes Showed Stronger Greening Trend than Equatorial-Facing Slopes in Tibetan Plateau Grasslands

Gaofei Yin[1], Xinyu Yan[1], Dujuan Ma[1], Jiangliu Xie[1], Rui Chen[1], Huiqin Pan[1], Wei Zhao[2], Changting Wang[3], Aleixandre Verger[4,5], Adrià Descals[5,6], Iolanda Filella[5,6], and Josep Peñuelas[5,6]

[1] Faculty of Geosciences and Environmental Engineering, Southwest Jiaotong University, Chengdu 610031, China

[2] Institute of Mountain Hazards and Environment, Chinese Academy of Sciences, Chengdu 610041, China

[3] Institute of Qinghai-Tibet Plateau, Southwest Minzu University, Chengdu 610041, China

[4] CIDE, CSIC-UV-GV, València 46113, Spain

[5] CREAF, Cerdanyola del Vallès, Barcelona 08193, Catalonia, Spain

[6] CSIC, Global Ecology Unit CREAF- CSIC- UAB, Bellaterra, Barcelona 08193, Catalonia, Spain

Corresponding author: Wei Zhao (zhaow@imde.ac.cn)

ABSTRACT

The orientation of slopes in alpine zones creates microclimates, e.g. equatorial-facing slopes (EFSs) are generally drier and warmer than are polar-facing slopes (PFSs). The vegetation growing in these microhabitats responds divergently to climatic warming depending on the slope orientation. We propose a spatial metric, the greenness asymmetric index (GAI), defined as the ratio between the average normalized difference vegetation index (NDVI) on PFSs and EFSs within a given spatial window, to quantify the asymmetry of greenness across aspects. We calculated GAI for each non-overlapping 3×3 km^2 (100×100 Landsat pixels) grid, and seamlessly mapped it on Tibetan Plateau (TP) grassland using NDVI time series from the Landsat-5, -7 and -8 satellites. PFSs were greener than EFSs (GAI > 1) in warm and dry areas, and EFSs were greener than PFSs (GAI < 1) in cold and wet areas. We also detected a stronger greening trend (0.0037 *vs* 0.0033 y^{-1}) and a higher sensitivity of NDVI to temperature (0.038 *vs* 0.033 ℃$^{-1}$) on PFSs than EFSs, leading to a significant positive trend in GAI (0.00062 y^{-1}, $P < 0.01$) in the TP from 1991 to 2020. Our results suggest that global warming exacerbated the greenness asymmetry associated with the slope orientation: PFSs are more sensitive to warming and have been greening at a faster rate than EFSs. The gradient of EFSs and PFSs provided a “natural laboratory” to study interaction of water and temperature limitations on vegetation growth. Our study is the first to detect the effect of aspect on the greening trend in the TP. Future research needs to clarify the full biotic and abiotic determinants for this spatial and temporal asymmetry of greenness across aspects with the support of extensive field measurements and refined high-resolution NDVI products.

KEYWORDS

Aspect gradient, greenness asymmetry, climatic warming, microclimate, greening, Tibetan Plateau

1. INTRODUCTION

Ecosystems at high latitudes and altitudes are strongly limited by low temperatures (Nemani et al., 2003; Seddon et al., 2016). Satellite observations indicate that cold-adapted vegetation under a warming climate experiences a substantial greening trend (Berner et al., 2020; Keenan and Riley, 2018; Myneni et al., 1997; Piao et al., 2020; Zhong et al., 2019). Latitude- and altitude-dependent warming further exacerbate this greening trend in cold regions (Pepin et al., 2015; Pithan and Mauritsen, 2014). Greening increases the amount of photosynthetically active radiation absorbed by vegetation and thus increases productivity (Piao et al., 2020). The recent prominent greening in cold regions has therefore exerted crucial influences on the temporal dynamics of atmospheric CO_2 concentrations. For example, the seasonal amplitude of CO_2 concentrations over the Northern Hemisphere has increased immensely since the 1950s (Forkel et al., 2016; Graven et al., 2013).

Whether the positive effect of warming on the growth of vegetation will continue in the predicted further warming, however, remains uncertain (Penuelas et al., 2017; Zhang et al., 2022). Recent studies have reported a slowing or even a reversal of greening in the Northern Hemisphere (Piao et al., 2014; Vickers et al., 2016; Zhang et al., 2021), which is often attributed to the approaching photosynthetic temperature optima (direct warming effects) (Duffy et al., 2021; Huang et al., 2019; Yin et al., 2022) and to the increase in other resource constraints with the mediation of temperature limitation, e.g. water constraints (indirect effects of warming) (Jiao et al., 2021; Yuan et al., 2019; Zhang et al., 2021). Examining the direct and indirect effects of warming on greenness across a wide spectrum of conditions of temperature and water availability using manipulative experiments is still rare due to their high cost, so the future trajectory of greenness under a warming climate remains unclear.

As an important topographic variable, aspect affects the amount and temporal cycle of solar radiation received by vegetation. This difference in radiation creates local microclimates with different temperatures and water availabilities (Bennie et al., 2008). Specifically, polar-facing slopes (PFSs) are generally wetter and colder than equatorial-facing slopes (EFSs) (Kumari et al., 2020). Aspect is therefore a key determinant of vegetation greenness. The contrast in greenness between EFSs and PFSs depends on the tradeoff between limitations of water and temperature (Kumari et al., 2020). An aspect gradient may therefore represent a natural laboratory for studying the codetermination of temperature and water availability on greenness. Most *in situ* measurements have indicated that vegetation grows better on PFSs than EFSs, especially for arid and semiarid ecosystems (Bale et al., 1998; Fekedulegn et al., 2003; Gong et al., 2008; Guerrero et al., 2016). Whether this phenomenon prevails at a regional scale, due to the sparse distribution of sampling sites, however, is still not clear. Studies have also not examined the interannual variation of the asymmetry of greenness across aspects, which is key to better understanding the responses of vegetation to warming.

Satellite-derived vegetation indices have been widely used to monitor the spatiotemporal dynamics of vegetation activity (An et al., 2018; Kumari et al., 2020; Yin et al., 2020). The normalized difference vegetation index (NDVI) was designed to represent the activity of vegetation based on information on the amounts of solar radiation absorbed by chlorophyll in the red band and scattered by mesophyll in the near-infrared band (Huete et al., 2002). NDVI is a reliable proxy for green biomass, with low sensitivity to many other confounding factors, e.g. topography and sun-observer geometry (Huete et al., 2002; Myneni et al., 1997; Shen et al., 2008). The Landsat satellites provide long-term (from 1972 to the present) and high-resolution (30 m) remotely sensed data (Wulder et al., 2019). The free delivery of the Landsat historical archive provides a novel opportunity to calculate NDVI and characterize the spatial pattern and interannual variation of aspect-dependent greenness over large areas at a higher spatial resolution and for a longer time record than do other satellites such as MODIS.

We used a spatial metric, the greenness asymmetric index (GAI), defined as the ratio of NDVIs for PFSs and EFSs, to quantify the asymmetry of greenness within a spatial window. We used long-term Landsat NDVI data, a digital elevation model (DEM) and a climatic data set to calculate GAI in each non-overlapping 3 × 3 km^2 (100 × 100 Landsat pixels) grid, mapped its spatial distribution and interannual variation in grassland on the Tibetan Plateau (TP) and explored their links to climate. The TP is the largest and highest plateau on Earth and is characterized by a cold and generally dry climate (Yao et al., 2019). Rapid warming has substantially increased the greenness of TP grassland (Zhong et al., 2019), but the effect of aspect on the spatiotemporal dynamics of greenness remains unknown. This study also deepens our understanding of the future trajectory of grassland greenness on the TP.

2. MATERIALS AND METHODS

2.1. Study area

The TP, also known as "the third pole of the Earth", is the largest and highest plateau in the world (Yao et al., 2019). Climate on the TP is generally characterized by low air temperatures and low precipitation, with the eastern TP is relatively warmer and wetter than western TP (Figure S1). Climatic warming on the TP has been intensive in recent decades, with a rate of about 0.03 ℃ y^{-1} (Figure S2a), which is nearly twice the global rate. This high rate of warming persisted even during the global "warming hiatus" period (An et al., 2018). Precipitation during this period also shows a significantly increasing trend (1.45 mm y^{-1}, $P = 0.03$. See Figure S2b).

Grass is the dominant type of vegetation on the TP (Figure 1a), where grassland greenness is co-controlled by temperature and water availability (Li et al., 2020; Shen et al., 2015). Rapid warming has significantly increased the greenness of TP grassland (Zhong et al., 2019). Topography on the TP is characterized by micro-relief (Figure 1b), so pairs of grasslands on EFSs and PFSs are readily available within a kilometric scale. The high rate of warming, relative homogeneous vegetation type and widely distributed micro-terrain make TP a suitable study area to assess the role of aspect in greenness (Figure 1) and its variation under ongoing climatic warming.

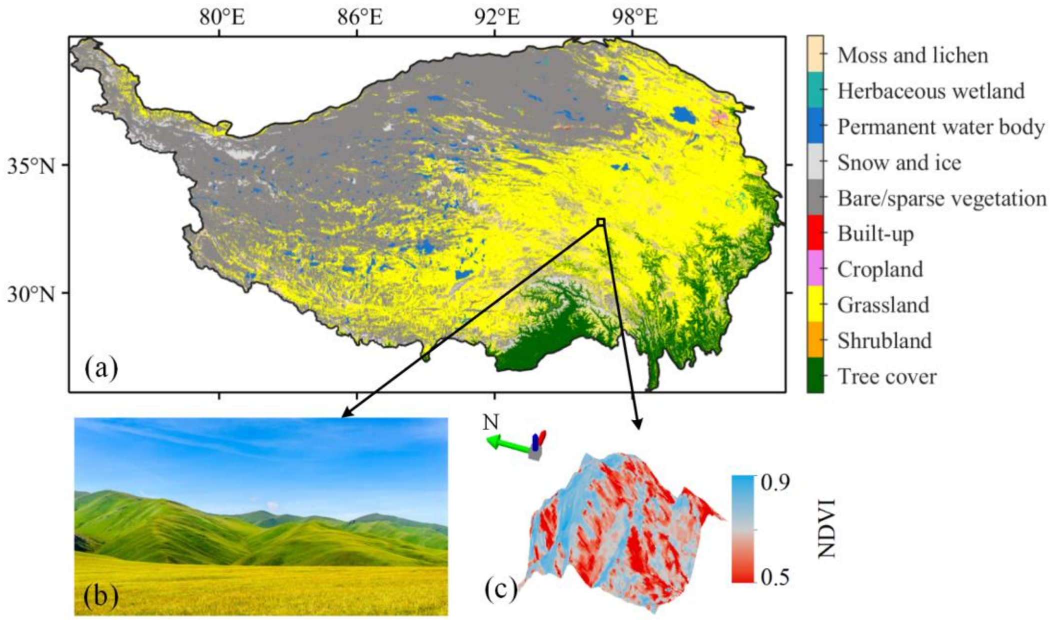

Figure 1 Land-cover type (a) and a typical landscape on the Tibetan Plateau (b) exemplifying micro-relief. (c) NDVI stacking on elevation in a 3 × 3 km^2 grid. In this case, NDVI on northward (polar-facing) slopes was larger than that on south-facing (equatorial-facing) slopes, resulting a greenness asymmetric index (GAI) value larger than 1.0 (see Analysis section). WorldCover, Landsat and GDEM data were used for the land cover, NDVI and elevation respectively (see the Data sets section).

2.2. Data sets

2.2.1. Landsat NDVI

We used Landsat-derived NDVI to represent the greenness of the grasslands. Landsat satellites provide the longest series of Earth observations using similar sensors with decametric resolutions (~30 m). All available observations of Landsat-5, -7 and -8 were used in this study, after masking out the cloud-contaminated observations identified by the CFMask algorithm (Zhu et al., 2015). NDVI was then calculated as the normalized difference between surface reflectances at near-infrared and red bands. For each pixel × year, we selected the maximum NDVI during July and August to represent the seasonal peak of greenness. This maximum compositing minimizes the influence of residual cloud and atmospheric contamination. All of the above preprocessing of the Landsat data was performed using the Google Earth Engine (GEE) platform (Gorelick et al., 2017). Code regarding the preprocessing can be found in https://code.earthengine.google.com/ec9fad54d1bc5071c13737fd784d9ccf?noload=true.

Landsat-5 and -7 have very similar spectral configurations, so their NDVIs are statistically the same (Claverie et al., 2015). Landsat-8, however, has narrower red and near-infrared bands, causing a positive bias for the derived NDVI relative to Landsat-5 and -7 (Roy et al., 2016). For consistency, we converted the Landsat-8 NDVI ($NDVI_{L8}$) to the Landsat-7 NDVI ($NDVI_{L7}$) by,

$$NDVI_{L7} = 0.0029+0.9589NDVI_{L8}. \quad (1)$$

The parameters in Eq. (1) were derived from a linear regression between 6317 $NDVI_{L8}$ and $NDVI_{L7}$ image pairs (Roy et al., 2016), which have been widely demonstrated to be reliable for long-term analyses of time series (Anderson et al., 2020; Fassnacht et al., 2019).

2.2.2. Gridded climatic data set

Gridded climatic data were obtained from the National Earth System Science Data Center of the National Science Technology Infrastructure of China (http://www.geodata.cn). This data set was reconstructed by scaling down the data from the Climatic Research Unit (CRU) at a resolution of 0.5° to a resolution of 1 km using data from 496 meteorological stations (Peng et al., 2019). We calculated the mean annual air temperature and mean annual precipitation from the original monthly resolution and resampled them to a spatial resolution of 3 km by averaging values of 3 × 3 pixels at the original resolution.

2.2.3. Land-cover data

We delineated TP grassland based on the WorldCover 10-m land-cover product of the European Space Agency (https://esa-worldcover.org/en). WorldCover was generated from Sentinel-1 and Sentinel-2 data with an overall accuracy of 74.4% (Zanaga et al., 2021). For consistency with the Landsat data, the WorldCover data were resampled to a resolution of 30 m using the nearest-neighbor method.

2.2.4. Elevational data

Elevational data were provided by the Advanced Spaceborne Thermal Emission and Reflection Radiometer Global Digital Elevation Model (GDEM) version 2 (http://www.jspacesystems.or.jp/ersdac/GDEM/E/1.html), which has a spatial resolution of 30 m. We calculated slopes and aspects for all pixels of the TP using GEE. Values of 0 and 180° in the aspect map correspond to north and south aspects, respectively. We identified pixels as EFSs when their slopes were >5° and their aspects were in the range of 135-225°. Similarly, PFSs pixels corresponded to pixels with slopes >5º and aspects in the range of 315-360° or 0-45°.

2.3. Analysis

We proposed GAI to quantify the asymmetry of greenness on contrasting aspects. GAI was calculated as,

$$GAI = NDVI_{PFS} / NDVI_{EFS} \quad (2)$$

where $NDVI_{PFS}$ and $NDVI_{EFS}$ are the maximum NDVI values during July and August on PFSs and EFSs, respectively. A GAI >1 indicates that PFSs are greener than EFSs. Contrarily, a GAI <1 indicates that EFSs are greener than PFSs.

Before calculating GAI, the original Landsat images were divided into non-overlapping 3×3 km^2 grids (100×100 Landsat pixels). The difference in vegetation type in each grid may induce uncertainty in GAI calculation, so only grassland pixel identified by the WorldCover product were selected for following processing. The grassland pixels on EFSs and PFSs were then extracted from each grid based on their definitions provided in Section 2.2.4. NDVIs for EFS and PFS were averaged to obtain $NDVI_{PFS}$ and $NDVI_{EFS}$, respectively, at a resolution of 3 km. Grid cells with <50 grassland pixels of valid Landsat data during July-August of either PFSs or EFSs were masked out to obtain a robust result. GAI was then calculated using Eq. (2) for each grid. This procedure generated one 3-km resolution GAI map, representing peak growing season, for each year. The TP started to be observed in 1986 by Landsat-5 (Pan et al., 2022). However, due to the low frequency of Landsat-5 acquisitions, the percentage of grids with available GAI values was very low (~50%) at the beginning of the time series and increased progressively with the combination of Landsat-5, -7 and -8 reaching percentages >90% after 1991 (Figure S3). To avoid possible issues introduced by the low number of valid estimates and to increase the robustness of the analysis, we therefore limited our study period to 1991-2020.

We first analyzed the spatiotemporal pattern of GAI relative to mean annual air temperature and mean annual precipitation. Collecting data for climatic variables to represent microclimatic conditions for each Landsat pixel at a decametric resolution is currently technically impossible, so we correlated GAI with both climatic variables at the 3-km resolution. We also compared the temporal trend and sensitivity of $NDVI_{PFS}$ and $NDVI_{EFS}$ to temperature for 1991 to 2020 to identify the influences of aspect on the response of greenness to climatic warming. The sensitivity of NDVI to temperature was calculated as the slope of the linear regression between NDVI and temperature (both at 3-km resolution). All trend statistics for GAI and NDVI were calculated using the linear regression of annual GAI and NDVI against year. All significance levels reported were estimated using a two-tailed Student's *t*-test.

3. RESULTS

3.1. Spatial pattern of greenness asymmetric index

Figure 2 shows the spatial distribution of mean GAI from 1991 to 2020. GAI was >1 in 63.6% of the grassland pixels, mainly in the western and northeastern TP. In contrast, fewer pixels (36.4%) had a GAI <1.0. These pixels were mostly in the eastern and central TP. Greenness generally differed significantly on the contrasting aspects (GAI $\neq$ 1) in 83.1% of the study area ($P < 0.01$) (Figure 2b).

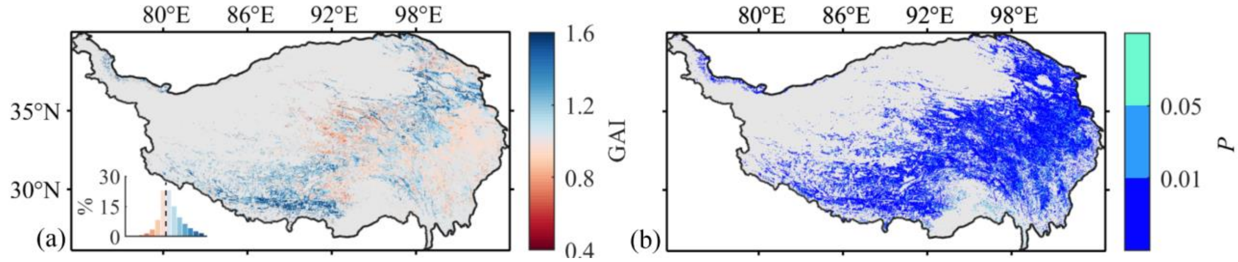

Figure 2 Spatial distribution of the average multiyear (1991-2020) (a) greenness asymmetric index (GAI) and (b) corresponding P values of the significant test results for mean GAI $\neq$ 1. P values are divided into three levels: P < 0.01, 0.01 < P < 0.05 and P > 0.05. Note that GAI > 1.0 represents greener polar-facing than equatorial-facing slopes and that GAI < 1.0 represents the opposite case. Gray background in the maps represent non-grassland land covers.

Putting GAI in a climatic space (Figure 3a) identified a significant correlation (P < 0.01) between GAI and both temperature (Figure 3b) and precipitation (Figure 3c), suggesting that GAI was co-determined by the ambient conditions of temperature and precipitation. This result indicated that PFSs were generally greener than EFSs in warm and dry areas and that the opposite case often occurred in cold and wet areas. Closer scrutiny indicated that precipitation (correlation coefficient = 0.93) was slightly more strongly correlated with the spatial pattern of GAI than was temperature (correlation coefficient = 0.91).

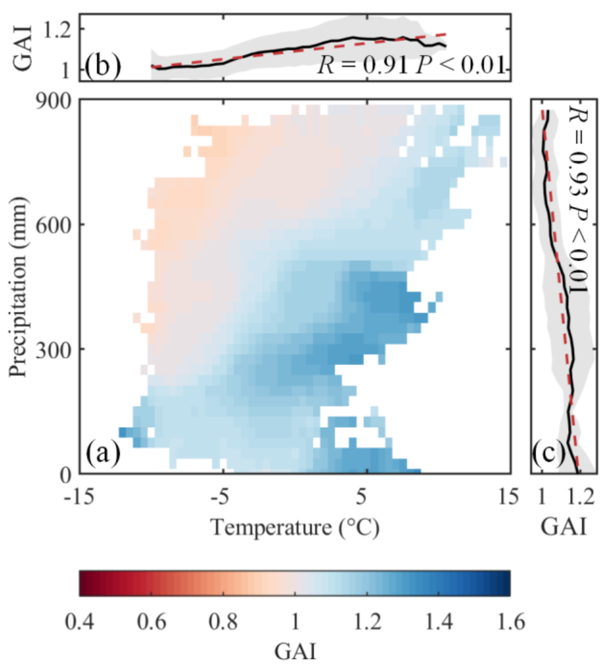

Figure 3 Distribution of the greenness asymmetric index (GAI) in the climatic space for TP grassland during 1991-2020. (a) GAI in each bin of mean annual temperature and mean annual precipitation. (b) GAI *vs* temperature, with GAI averaged over all precipitation bins. (c) GAI *vs* precipitation, with GAI averaged over all temperature bins.

3.2. Divergent greening rates on equatorial-facing and polar-facing slopes

The regional mean GAI significantly ($P < 0.01$) increased from 1991 to 2020 at a rate of 0.00065 y^{-1} (Figure 4), albeit with obvious spatial heterogeneity (Figure 5). Specifically, GAI increased in 60.4% of the study area, and the increasing trend was significant in 39.6% of the study area at $P < 0.01$, mainly in eastern and central TP. In contrast, GAI decreased significantly in only 15.1% of the pixels ($P < 0.01$), distributed mainly in northeastern TP.

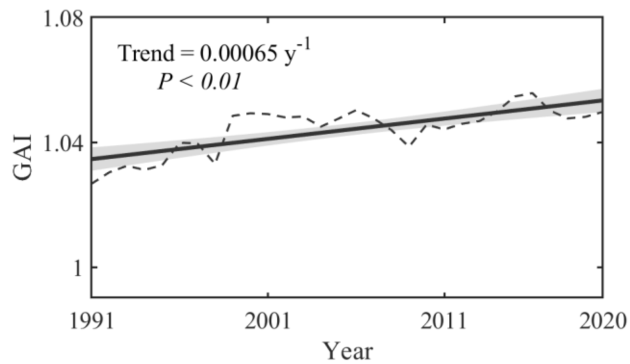

Figure 4 Temporal trend of the greenness asymmetric index (GAI) averaged over the entire Tibetan Plateau. The solid line and shaded area represent the linear regression and 95% confidence limit of the estimated slope, respectively.

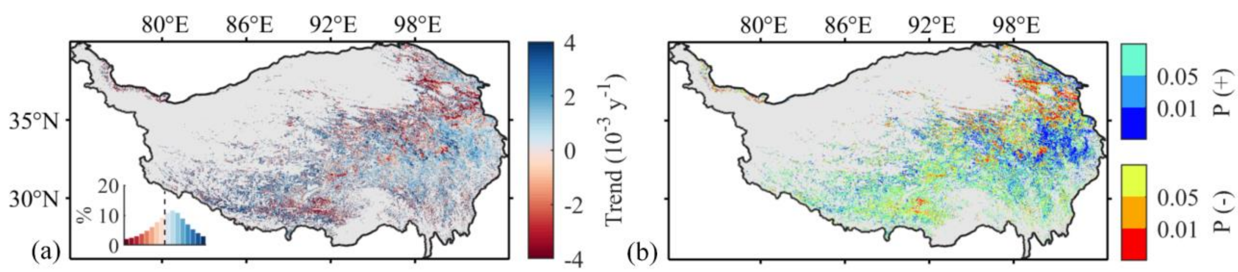

Figure 5 Spatial distribution of the trend in the greenness asymmetric index (GAI) and its significant test results from 1991 to 2020 for the Tibetan Plateau. P(+) and P(-) are the P values of the increase and decrease in GAI, respectively, which are divided into three levels: $P < 0.01$, $0.01 < P < 0.05$ and $P > 0.05$. Gray background in the maps represent non-grassland land covers.

The increase in GAI implied that the greening rate on PFSs may outpace the rate on EFSs. We therefore compared the temporal trends in NDVI on the two opposite aspects. NDVI significantly increased ($P < 0.01$) from 1991 to 2020 on both aspects, but at different rates: 0.0040 and 0.0034 y^{-1} for PFSs and EFSs, respectively (Figure 6). The spatial distributions of the NDVI trend on the two contrasting aspects confirmed the significant greening trend for the entire TP (Figure S4a and c). This greening trend was significant ($P < 0.01$) in 77.6 and 83.3% of all pixels for the EFSs and PFSs, respectively (Figure S4b and d). We further mapped the pixel-wise difference in NDVI trends between the EFSs and PFSs for the entire TP (Figure 7) and observed widespread positive values (67.7% of all pixels, Figure 7a), i.e. PFSs benefited more from climate change than did EFSs. A two-tailed Student's *t*-test for all pairs of EFSs and PFSs confirmed a significant difference in the greening rates between the two contrasting aspects at $P < 0.01$ (Figure 7b).

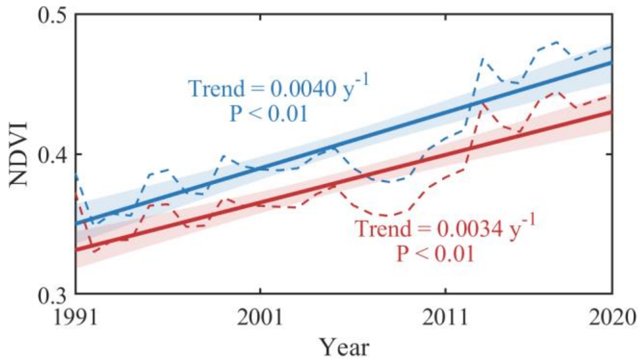

Figure 6 Temporal trends in the average NDVI on equatorial-facing (red lines) and polar-facing (blue lines) slopes from 1991 to 2020 on the Tibetan Plateau grasslands. The solid lines and shaded areas represent the linear regressions and 95% confidence limits of the estimated slopes, respectively.

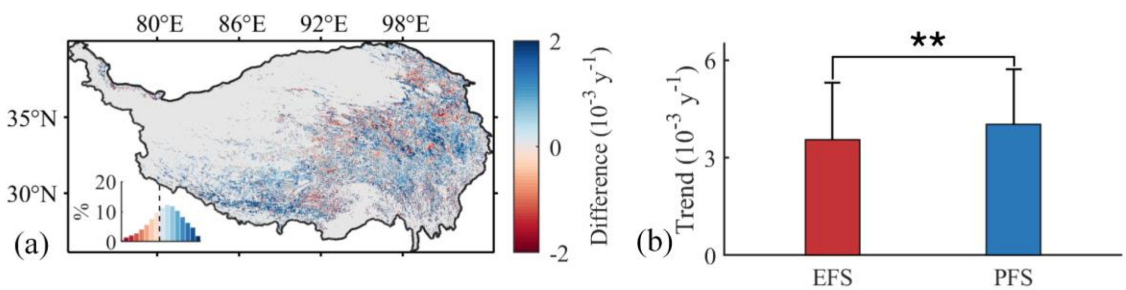

Figure 7 Spatial distribution of the difference in NDVI trends between polar-facing (PFSs) and equatorial-facing slopes (EFSs) (a) and their box plots (b). Gray background in (a) represent non-grassland land covers. The asterisks in (b) indicate a significant difference in the greening trends between the equatorial-facing (EFSs) and polar-facing slopes (PFSs) at $P < 0.01$. The error bars indicate standard errors of the means.

Finally, we compared the apparent sensitivity of NDVI to temperature (S_T) between EFSs and PFSs to directly determine whether the aspect would regulate the response of greenness to warming. We detected a widespread positive S_T of NDVI on both the EFSs and PFSs, accounting for 88.4 and 90.6% of their total pixels, respectively (Figure S5a and c). A positive S_T was significant ($P < 0.01$) in 21.9 and 27.4% of the pixels for the EFSs and PFSs, respectively, mostly in the eastern TP (Figure S5b and d). A map of the difference in S_T on the two contrasting aspects indicated that S_T was generally higher for PFSs (Figure 8a). The regional mean S_T was accordingly significantly ($P < 0.01$) higher on PFSs than EFSs (0.031 ± 0.025 *vs* 0.026 ± 0.025 ℃^{1}, mean ± σ). These results suggest that PFSs would benefit more than EFSs from the ongoing warming.

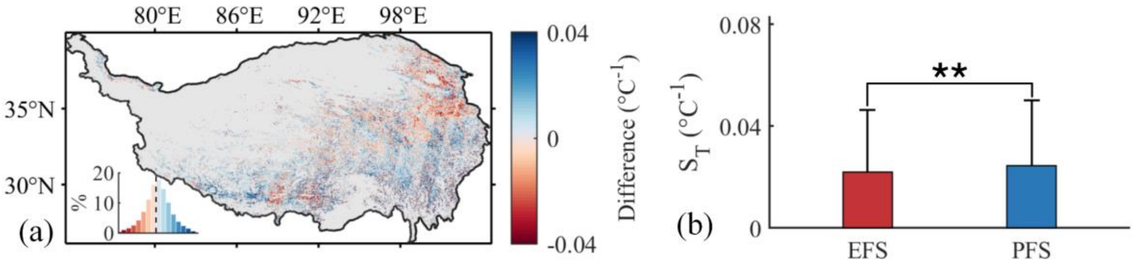

Figure 8 Spatial distribution of the difference in apparent sensitivity of NDVI to temperature (S_T) between polar-facing (PFSs) and equatorial-facing slopes (EFSs) (a) and their box plots (b). S_T is defined as the slope of the linear regression between NDVI and temperature for 1991-2020. Gray background in (a) represent non-grassland land covers. The asterisks in (b) indicate a significant difference in the NDVI rates between the equatorial-facing (EFSs) and polar-facing slopes (PFSs) at $P < 0.01$. The error bars indicate standard errors of the means.

4. DISCUSSION

Different orientations of EFSs and PFSs generate contrasting microclimatic conditions that influence vegetation growth and its response to climate change (Dobrowski, 2011). Our findings validate the previously sparsely tested observations of widespread differences in greenness between EFSs and PFSs (Bale et al., 1998; Fekedulegn et al., 2003; Gong et al., 2008; Guerrero et al., 2016). The variation in greenness between EFSs and PFSs depends on the relative importance of temperature and water limitations in shaping regional vegetation growth. PFSs exhibit higher greenness (GAI > 1) in water-limited areas and was lower greenness than EFSs (GAI < 1) in temperature-limited areas (Figure 3). The GAI threshold of 1 represents the transition point between temperature and water limitations. The distinct spatial pattern of GAI, suggests that western TP (GAI >1) is primarily limited by water, while the eastern TP (GAI <1) predominantly limited by temperature, which is consistent with a recent study (Zhu et al., 2023). This indicates that GAI can serve as a reliable metric for quantifying water and temperature limitations of in an ecosystem. We also observed an increasing trend in GAI from 1991 to 2020, indicating a stronger influence of water constraints relative to temperature constraints on the TP grasslands, despite the concurrent warming and wetting trends in the region (see Figure S2). Ding et al. (2018) also reported a similar shift in climatic constraints on vegetation growth over the TP using direct correlation analysis between climatic variables and vegetation growth.

The warming climate has caused a greening trend in areas at high latitudes and altitudes, where vegetation growth is mainly constrained by low temperatures (Berner et al., 2020; Keenan and Riley, 2018; Myneni et al., 1997; Zhong et al., 2019). Recent studies, however, have reported that this greening trend may slow or even reverse with continuous warming (Yin et al., 2022; Yuan et al., 2019; Zhang et al., 2022). One potential mechanism underlying these findings is the regulation of water availability on vegetation response to warming. Warming can stimulate vegetation growth under wet conditions but suppress it under extremely dry conditions (Quan et al., 2019; Reich et al., 2018). By comparing the vegetation response to warming under wet and dry conditions while controlling for other confounding environmental factors, we can enhance our ability to predict vegetation dynamics in future climates. EFSs and PFSs, distinguished by differences in solar energy exposure, lead to different rates of water vapor release through evapotranspiration. The increased solar input on EFSs enhances their capability to emit water vapor, leading to drier conditions compared to the relatively lower moisture loss in PFSs. As a result, EFSs and PFSs, representing dry and wet conditions respectively within comparable regional ambient climates, function as a "natural laboratory" for comparing vegetation responses to warming under distinct moisture regimes. The larger increasing trend (Figure 7) and the apparent temperature sensitivity of NDVI in PFSs compared to EFSs (Figure 8) support the regulation of water availability on vegetation response to warming.

In addition to background climate, other factors, including slope steepness, community composition, soil nutrient content and orographic precipitation, may influence the spatiotemporal pattern of GAI. We compared GAI maps derived from different slope ranges (Figure S6), finding that GAIs calculated from gentle slopes are much more concentrated around 1, and the steeper slopes would result in GAI with a higher absolute value, i.e., steeper slope would amplify the aspect effect on vegetation greenness. For community composition, EFSs and PFSs are generally dominated by drought-tolerant and cold-adapted species, respectively (Kimball et al., 2017). Plant species have also shifted from EFSs to PFSs in recent decades due to climatic warming, increasing biodiversity on PFSs (Feldmeier et al., 2020). This species shift in aspect may also account for the larger greening trend on PFSs because of the positive relationship between biodiversity and biomass production (Sonkoly et al., 2019; Tilman et al., 1996). The more-fertile soil on PFSs than EFSs (Kumari et al., 2020) is also a potential cause of the stronger greening trend, due to the high nutrient limitation on the TP (Liu et al., 2018). Furthermore, the orographic precipitation also plays a role in regulating the aspect-controlled vegetation growth, as demonstrated by computer simulations in a recent study (Srivastava et al., 2022). Theses local-scale factors besides climate controls may induce local variations in GAI, as can be discerned in the spatiotemporal distributions of GAI (Figure 2 and 5). Therefore, extensive *in situ* measurements are required to identify all biotic and abiotic factors creating the contrasting trends of greenness and greening on EFSs and PFSs on the TP.

Our results have some uncertainties. First, we used NDVI as a proxy of vegetation greenness, because our previous study demonstrated that the topographic influence on NDVI could be neglected due to its formulation of normalized ratios (Chen et al., 2020). To avoid the topographic effects on NDVI, only slopes larger than 5° and lower than 25° were selected in a similar study (Kumari et al., 2020). However, since the two GAI maps, respectively calculated from pixels with slopes larger than 5° and in the range of 5°-25°, are broadly similar (Figure S7), the uncertainty caused by topographic effects on NDVI is thus very limited and does not significantly influence our results. Second, we focused on summer greenness, which is assumed to well represent the variation in annual gross primary productivity (Xia et al., 2015). The symmetricity of greenness may exhibit seasonal variation as revealed in (Kumari et al., 2020). We compared the GAI in grassland growing seasons, i.e., spring, summer and autumn (Figure S8), and found that the spatial patterns in the three seasons are very similar. Third, the detailed biotic and abiotic differences between EFSs and PFSs cannot be specified without the support of extensive field measurements, including meteorological conditions, soil properties and community composition. Dedicated field campaigns are urgently needed on paired EFSs and PFSs at representative sites on the plateau. Forth, Landsat satellites have a relatively low revisiting frequency (~16 days), and cloud contamination further lowers the number of high-quality observations, causing uncertainty associated with NDVI. Advanced spatiotemporal fusion technology may improve the continuity of NDVI time series for refining our results. Finally, the east and west facing slopes may also exhibit different greenness due to diurnal cycle of convective system, so the greenness difference between these two contrasting slopes is also worth comparing in our future study.

5. Conclusions

Our study presents a novel approach, using the greenness asymmetric index (GAI), to seamlessly map the divergence in greenness between equatorial-facing slopes (EFSs) and polar-facing slopes (PFSs) in the Tibetan Plateau (TP) grasslands. This widespread distribution of greenness divergence across the TP can be attributed to the varying influences of water and temperature limitations. Our analysis also revealed an increasing trend in GAI from 1991 to 2020, indicating a growing significance of water constraints compared to temperature constraints on the TP. The gradients provided by EFSs and PFSs offer a valuable "natural laboratory" for furthering our mechanistic understanding of vegetation response to climate change, thereby enhancing the representation of Earth system models and improving predictions of future vegetation dynamics. Future studies should focus on dedicated field measurements and refined high-resolution NDVI products to elucidate the complete range of biotic and abiotic factors contributing to the spatiotemporal patterns of GAI.

ACKNOWLEDGMENTS

This study was funded by the National Natural Science Foundation of China 42271323 and 41971282, the Sichuan Science and Technology Program 2021JDJQ0007, the Spanish Government project TED2021-132627B-I00 funded by the Spanish MCIN, AEI/10.13039/501100011033 and the European Union NextGenerationEU/PRTR, the Fundación Ramón Areces project CIVP20A6621 and the Catalan government project SGR2021-1333. This study represents a contribution to CSIC-PTI TELEDETECT.

CONFLICT OF INTEREST

The authors declare no conflicts of interest.

SUPPLEMENTARY INFORMATION

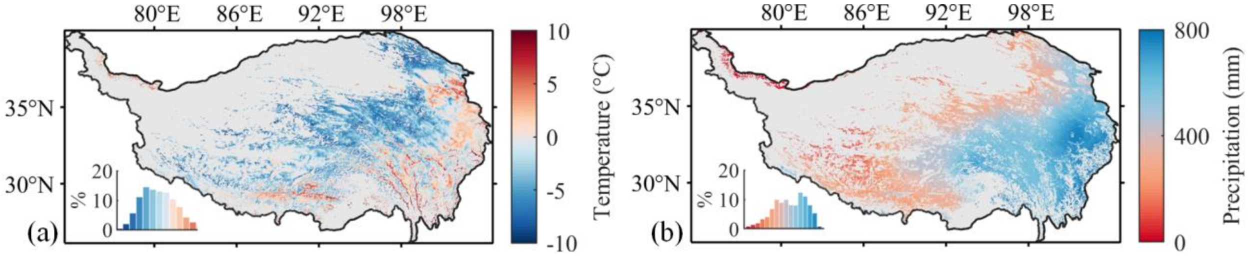

Figure S1 Spatial distribution of the mean annual temperature and mean annual precipitation on the Tibetan Plateau grasslands. Gray background in the maps represent non-grassland land covers.

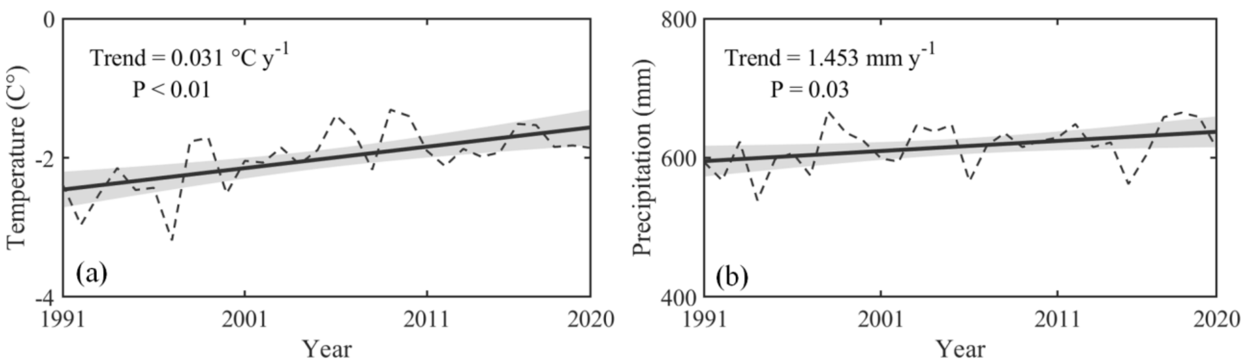

Figure S2 Temporal trends in the mean annual temperature and mean annual precipitation from 1991 to 2020 averaged over the Tibetan Plateau. The solid lines and shaded areas represent the linear regressions and 95% confidence limits of the estimated slopes, respectively.

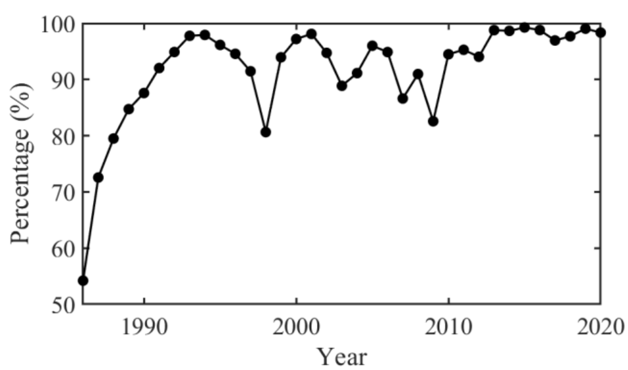

Figure S3 Temporal variation in the percentage of grids with greenness asymmetric index (GAI) values. Due to Landsat acquisition and cloud contamination, the percentage before 1991 was very low (< 85%), we therefore limited our study period to 1991-2020.

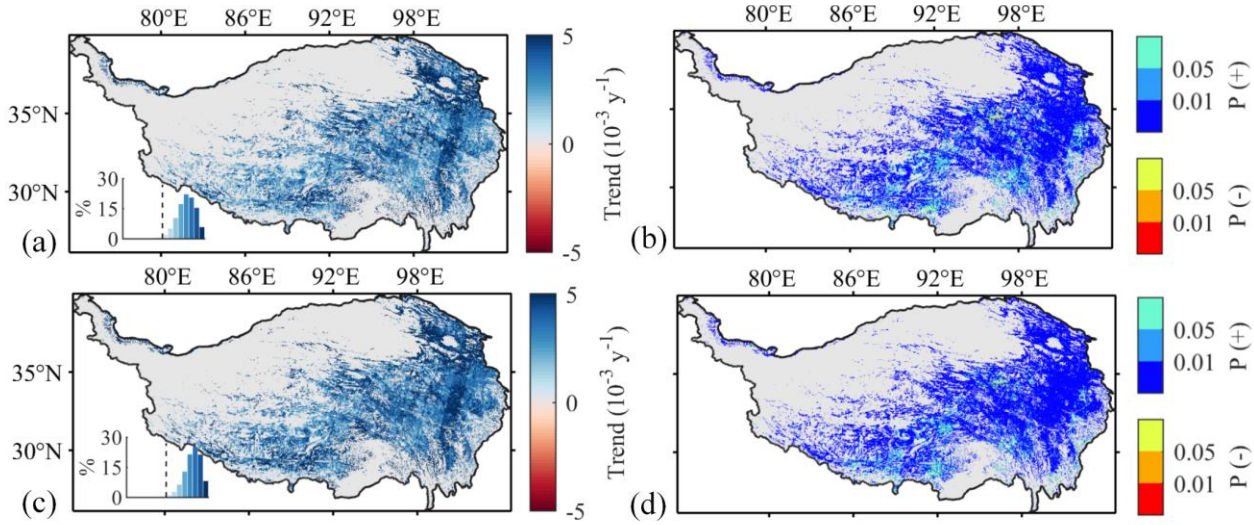

Figure S4 Spatial distribution of the trend in summer NDVI and its significant test results for 1991 to 2020 on the Tibetan Plateau grasslands. Panels (a) and (b) are for equatorial-facing slopes, and panels (c) and (d) are for polar-facing slopes. P(+) and P(-) in (b) and (d) are the *P* values of the increase and decrease in NDVI, respectively, which are divided into three levels: $P < 0.01$, $0.01 < P < 0.05$ and $P > 0.05$. Gray background in the maps represent non-grassland land covers.

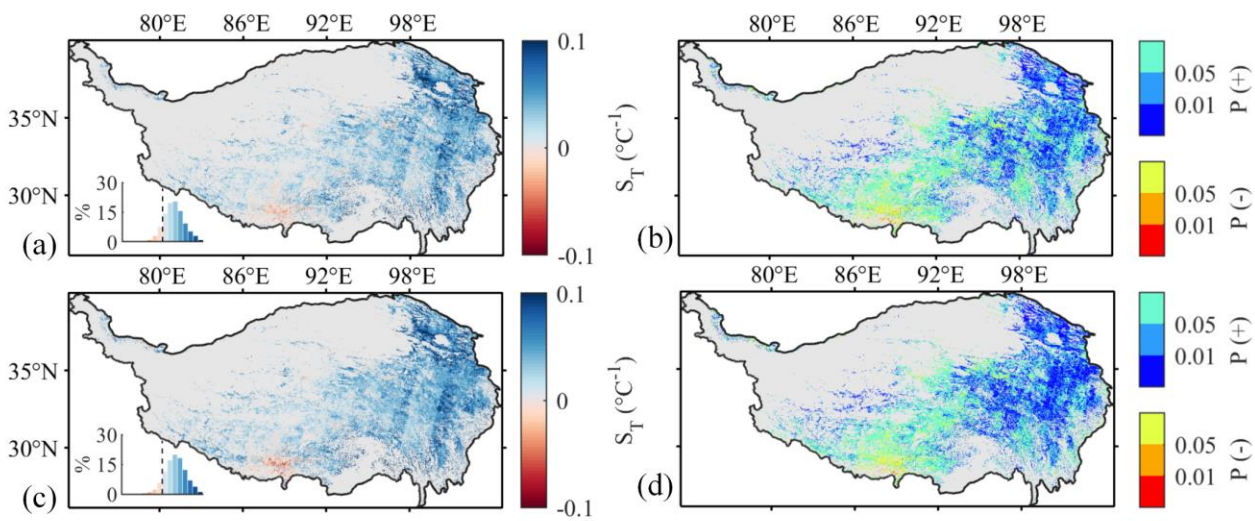

Figure S5 Spatial distribution of the sensitivity of greenness to temperature (S_T) and its significant test results for the Tibetan Plateau grasslands. Panels (a) and (b) are for equatorial-facing slopes, and panels (c) and (d) are for polar-facing slopes. S_T is defined as the slope of the linear regression between NDVI and temperature for 1991-2020. P(+) and P(-) are the *P* values of positive and negative S_T, respectively, which are divided into three levels: $P < 0.01$, $0.01 < P < 0.05$ and $P > 0.05$. Gray background in the maps represent non-grassland land covers.

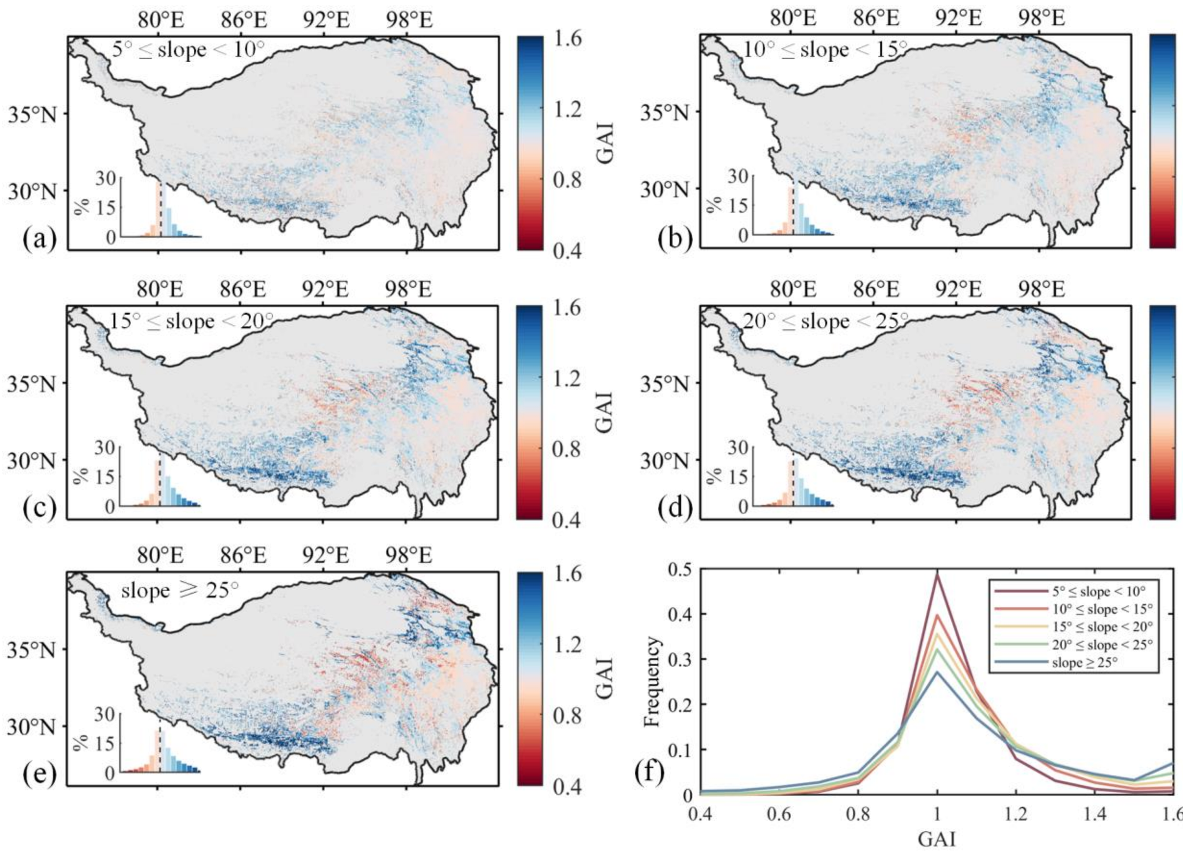

Figure S6 Spatial distributions of the greenness asymmetric index (GAI) calculated with different slope ranges: 5°-10° (a), 10°-15° (b), 15°-20° (c), 20°-25° (d) and > 25° (e), and their frequency distribution (f). Note that GAI > 1.0 represents greener polar-facing than equatorial-facing slopes and that GAI < 1.0 represents the opposite case. Gray background in the maps represent non-grassland land covers.

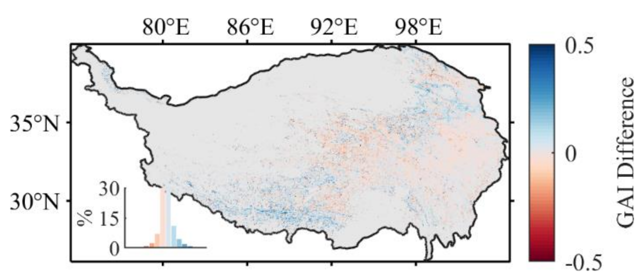

Figure S7 Difference between greenness asymmetric indexes (GAIs) calculated from pixels with slopes > 5° and with slopes in the range of 5°-25°, respectively. There was no significant difference between their bias and 0 ($P < 0.01$). Gray background in the maps represent non-grassland land covers.

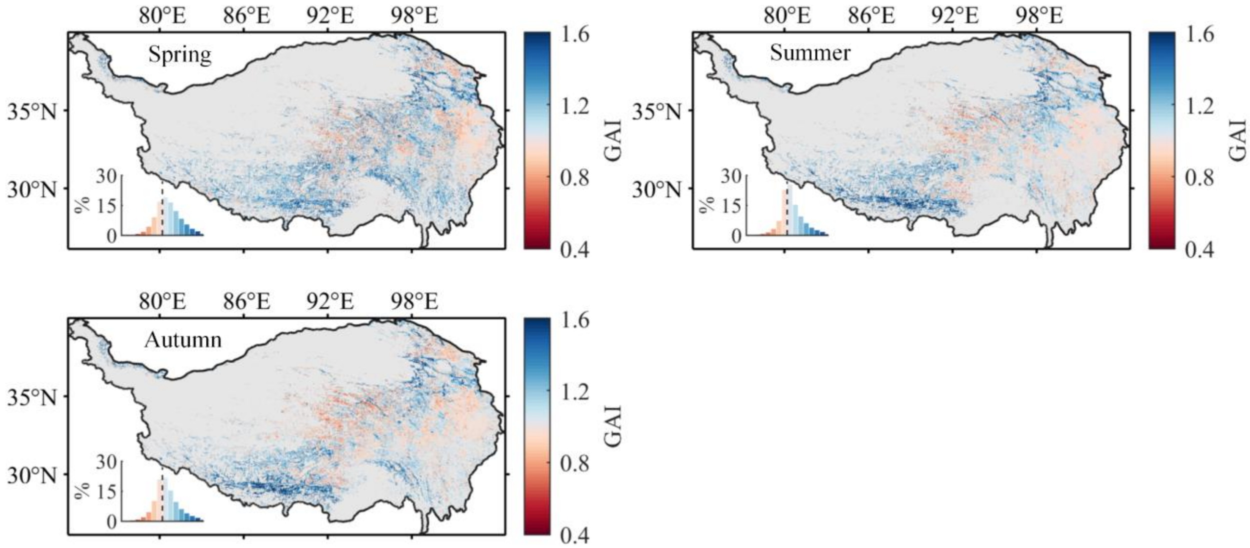

Figure S8 Spatial distribution of the greenness asymmetric index (GAI) in spring (May and June), summer (July and August) and autumn (September and October). Note that GAI > 1.0 represents greener polar-facing than equatorial-facing slopes and that GAI < 1.0 represents the opposite case. Gray background in the maps represent non-grassland land covers.

REFERENCES

An, S. et al., 2018. Mismatch in elevational shifts between satellite observed vegetation greenness and temperature isolines during 2000-2016 on the Tibetan Plateau. Global Change Biology, 24(11): 5411-5425.

Anderson, K. et al., 2020. Vegetation expansion in the subnival Hindu Kush Himalaya. Global Change Biology, 26(3): 1608-1625.

Bale, C.L., Williams, J.B. and Charley, J.L., 1998. The impact of aspect on forest structure and floristics in some Eastern Australian sites. Forest Ecology and Management, 110(1-3): 363-377.

Bennie, J., Huntley, B., Wiltshire, A., Hill, M.O. and Baxter, R., 2008. Slope, aspect and climate: Spatially explicit and implicit models of topographic microclimate in chalk grassland. Ecological Modelling, 216(1): 47-59.

Berner, L.T. et al., 2020. Summer warming explains widespread but not uniform greening in the Arctic tundra biome. Nature Communications, 11(1): 4621.

Chen, R., Yin, G.F., Liu, G.X., Li, J. and Verger, A., 2020. Evaluation and Normalization of Topographic Effects on Vegetation Indices. Remote Sensing, 12(14).

Claverie, M., Vermote, E.F., Franch, B. and Masek, J.G., 2015. Evaluation of the Landsat-5 TM and Landsat-7 ETM + surface reflectance products. Remote Sensing of Environment, 169: 390-403.

Dobrowski, S.Z., 2011. A climatic basis for microrefugia: the influence of terrain on climate. Global Change Biology, 17(2): 1022-1035.

Duffy, K.A. et al., 2021. How close are we to the temperature tipping point of the terrestrial biosphere? Science Advances, 7(3).

Fassnacht, F.E., Schiller, C., Kattenborn, T., Zhao, X.Q. and Qu, J.P., 2019. A Landsat-based vegetation trend product of the Tibetan Plateau for the time-period 1990-2018. Scientific Data, 6.

Fekedulegn, D., Hicks, R.R. and Colbert, J.J., 2003. Influence of topographic aspect, precipitation and drought on radial growth of four major tree species in an Appalachian watershed. Forest Ecology and Management, 177(1-3): 409-425.

Feldmeier, S. et al., 2020. Shifting aspect or elevation? The climate change response of ectotherms in a complex mountain topography. Diversity and Distributions, 26(11): 1483-1495.

Forkel, M. et al., 2016. Enhanced seasonal CO2 exchange caused by amplified plant productivity in northern ecosystems. Science, 351(6274): 696-9.

Gong, X. et al., 2008. Slope aspect has effects on productivity and species composition of hilly grassland in the Xilin River Basin, Inner Mongolia, China. Journal of Arid Environments, 72(4): 483-493.

Gorelick, N. et al., 2017. Google Earth Engine: Planetary-scale geospatial analysis for everyone. Remote Sensing of Environment, 202: 18-27.

Graven, H.D. et al., 2013. Enhanced Seasonal Exchange of CO2 by Northern Ecosystems Since 1960. Science, 341(6150): 1085-1089.

Guerrero, F.J.D., Hinojosa-Corona, A. and Kretzschmar, T.G., 2016. A Comparative Study of NDVI Values Between North- and South-Facing Slopes in a Semiarid Mountainous Region. IEEE Journal of Selected Topics in Applied Earth Observations and Remote Sensing, 9(12): 5350-5356.

Huang, M.T. et al., 2019. Air temperature optima of vegetation productivity across global biomes. Nature Ecology & Evolution, 3(5): 772-779.

Huete, A. et al., 2002. Overview of the radiometric and biophysical performance of the MODIS vegetation indices. Remote Sensing of Environment, 83(1-2): 195-213.

Jiao, W.Z. et al., 2021. Observed increasing water constraint on vegetation growth over the last three decades. Nature Communications, 12(1).

Keenan, T.F. and Riley, W.J., 2018. Greening of the land surface in the world's cold regions consistent with recent warming. Nature Climate Change, 8(9): 825-+.

Kimball, S., Lulow, M.E., Balazs, K.R. and Huxman, T.E., 2017. Predicting drought tolerance from slope aspect preference in restored plant communities. Ecology and Evolution, 7(9): 3123-3131.

Kumari, N. et al., 2020. The Grass Is Not Always Greener on the Other Side: Seasonal Reversal of Vegetation Greenness in Aspect-Driven Semiarid Ecosystems. Geophysical Research Letters, 47(15): e2020GL088918.

Li, P.L., Hu, Z.M. and Liu, Y.W., 2020. Shift in the trend of browning in Southwestern Tibetan Plateau in the past two decades. Agricultural and Forest Meteorology, 287.

Liu, S.B., Zamanian, K., Schleuss, P.M., Zarebanadkouki, M. and Kuzyakov, Y., 2018. Degradation of Tibetan grasslands: Consequences for carbon and nutrient cycles. Agriculture Ecosystems & Environment, 252: 93-104.

Myneni, R.B., Keeling, C.D., Tucker, C.J., Asrar, G. and Nemani, R.R., 1997. Increased plant growth in the northern high latitudes from 1981 to 1991. Nature, 386(6626): 698-702.

Nemani, R.R. et al., 2003. Climate-driven increases in global terrestrial net primary production from 1982 to 1999. Science, 300(5625): 1560-3.

Pan, Y.H. et al., 2022. Characteristics of Greening along Altitudinal Gradients on the Qinghai-Tibet Plateau Based on Time-Series Landsat Images. Remote Sensing, 14(10).

Peng, S.Z., Ding, Y.X., Liu, W.Z. and Li, Z., 2019. 1 km monthly temperature and precipitation dataset for China from 1901 to 2017. Earth System Science Data, 11(4): 1931-1946.

Penuelas, J. et al., 2017. Shifting from a fertilization-dominated to a warming-dominated period. Nature Ecology & Evolution, 1(10): 1438-1445.

Pepin, N. et al., 2015. Elevation-dependent warming in mountain regions of the world. Nature Climate Change, 5(5): 424-430.

Piao, S.L. et al., 2014. Evidence for a weakening relationship between interannual temperature variability and northern vegetation activity. Nature Communications, 5.

Piao, S.L. et al., 2020. Characteristics, drivers and feedbacks of global greening. Nature Reviews Earth & Environment, 1(1): 14-27.

Pithan, F. and Mauritsen, T., 2014. Arctic amplification dominated by temperature feedbacks in contemporary climate models. Nature Geoscience, 7(3): 181-184.

Quan, Q. et al., 2019. Water scaling of ecosystem carbon cycle feedback to climate warming. Science Advances, 5(8).

Reich, P.B. et al., 2018. Effects of climate warming on photosynthesis in boreal tree species depend on soil moisture. Nature, 562(7726): 263-+.

Roy, D.P. et al., 2016. Characterization of Landsat-7 to Landsat-8 reflective wavelength and normalized difference vegetation index continuity. Remote Sensing of Environment, 185: 57-70.

Seddon, A.W.R., Macias-Fauria, M., Long, P.R., Benz, D. and Willis, K.J., 2016. Sensitivity of global terrestrial ecosystems to climate variability. Nature, 531(7593): 229-+.

Shen, M. et al., 2008. Estimation of aboveground biomass using in situ hyperspectral measurements in five major grassland ecosystems on the Tibetan Plateau. Journal of Plant Ecology, 1(4): 247-257.

Shen, M.G., Piao, S.L., Cong, N., Zhang, G.X. and Janssens, I.A., 2015. Precipitation impacts on vegetation spring phenology on the Tibetan Plateau. Global Change Biology, 21(10): 3647-3656.

Sonkoly, J. et al., 2019. Both mass ratio effects and community diversity drive biomass production in a grassland experiment. SCIENTIFIC REPORTS, 9.

Srivastava, A. et al., 2022. Influence of orographic precipitation on coevolving landforms and vegetation in semi-arid ecosystems. Earth Surface Processes and Landforms, 47(12): 2846-2862.

Tilman, D., Wedin, D. and Knops, J., 1996. Productivity and sustainability influenced by biodiversity in grassland ecosystems. Nature, 379(6567): 718-720.

Vickers, H. et al., 2016. Changes in greening in the high Arctic: insights from a 30 year AVHRR max NDVI dataset for Svalbard. Environmental Research Letters, 11(10).

Wulder, M.A. et al., 2019. Current status of Landsat program, science, and applications. Remote Sensing of Environment, 225: 127-147.

Xia, J.Y. et al., 2015. Joint control of terrestrial gross primary productivity by plant phenology and physiology. Proceedings of the National Academy of Sciences of The United States of America, 112(9): 2788-2793.

Yao, T.D. et al., 2019. Recent Third Pole's Rapid Warming Accompanies Cryospheric Melt and Water Cycle Intensification and Interactions between Monsoon and Environment: Multidisciplinary Approach with Observations, Modeling, and Analysis. Bulletin of the American Meteorological Society, 100(3): 423-444.

Yin, G., Verger, A., Filella, I., Descals, A. and Peñuelas, J., 2020. Divergent Estimates of Forest Photosynthetic Phenology Using Structural and Physiological Vegetation Indices. Geophysical Research Letters, 47(18).

Yin, G.F., Verger, A., Descals, A., Filella, I. and Penuelas, J., 2022. Nonlinear Thermal Responses Outweigh Water Limitation in the Attenuated Effect of Climatic Warming on Photosynthesis in Northern Ecosystems. Geophysical Research Letters, 49(16).

Yuan, W.P. et al., 2019. Increased atmospheric vapor pressure deficit reduces global vegetation growth. Science Advances, 5(8).

Zanaga, D. et al., 2021. ESA WorldCover 10 m 2020 v100.

Zhang, A.Z., Jia, G.S. and Ustin, S.L., 2021. Water availability surpasses warmth in controlling global vegetation trends in recent decade: revealed by satellite time series. Environmental Research Letters, 16(7).

Zhang, Y.C. et al., 2022. Future reversal of warming-enhanced vegetation productivity in the Northern Hemisphere. Nature Climate Change, 12(6): 581-+.

Zhong, L., Ma, Y.M., Xue, Y.K. and Piao, S.L., 2019. Climate Change Trends and Impacts on Vegetation Greening Over the Tibetan Plateau. Journal of Geophysical Research-Atmospheres, 124(14): 7540-7552.

Zhu, Z. et al., 2023. Optimality principles explaining divergent responses of alpine vegetation to environmental change. Global Change Biology, 29(1): 126-142.

Zhu, Z., Wang, S.X. and Woodcock, C.E., 2015. Improvement and expansion of the Fmask algorithm: cloud, cloud shadow, and snow detection for Landsats 4-7, 8, and Sentinel 2 images. Remote Sensing of Environment, 159: 269-277.